Acta Mechanica Slovaca **27 (3): 28- 40,** September **2023**
https://doi.org/10.21496/ams.2023.026

Acta Mechanica Slovaca
ISSN 1335-2393
www.actamechanica.sk

Effects of Welding Sequences on Residual Stresses in a Butt Joint of Austenitic Piping

Chouaib Zeghida [1*], Abdelmoumene Guedri [1]

[1] Infra-Res Laboratory, Department of Mechanical Engineering, University of Souk Ahras, Souk Ahras, Algeria

Abstract: This study aimed to investigate the effects of welding sequences on residual stresses and distortions of welded components, using computational thermomechanical model-based finite element analysis (FEA). Residual stresses, a common outcome of welding, can cause material distortions and reduce product quality. We used FEA to simulate transient temperature fields generated during welding and evaluated their impact on the amplitude and distribution of residual stresses, the size of fusion and heat-affected zones, material microstructures, properties and fracture toughness. The study focused on an austenitic pipe butt junction, a commonly welded component in various industries. The identification of optimal welding sequences can minimize residual stresses and distortions, providing valuable insights for the development of efficient welding techniques, improved product quality, and reduced manufacturing costs.

Keywords: Welding sequences, Residual stresses, Distortions, Finite element analysis, Austenitic piping.

1. Introduction

Welding is a complex process that involves the application of intense localized heating followed by rapid cooling, which creates significant thermal stress gradients around the joint. These thermal stresses can cause deformation and cracking in the weld, which can compromise the structural integrity and functionality of the component. As discussed by Withers et al. [1], the transient temperature field created during welding can make the welded structure vulnerable to hydrogen embrittlement and other negative effects. Therefore, understanding the temperature evolution and thermal behaviour of welded structures is crucial, particularly in high-integrity steel components, as the heat source can cause microstructural changes that may lead to a loss of structural integrity.

Popular techniques like Finite Element Analysis (FEA) are used to simulate welding processes, but their efficacy is constrained by the intricate connections between thermal, mechanical, and metallurgical processes that are involved in welding [2-4]. Researchers have developed different models to address these challenges, Hibbitt et al. [5] used a highly focused heat source in motion to address a heat transfer issue when conducting a thermal evaluation of a welding operation. One of the most widely used heat source models in welding analysis is the moving double ellipsoidal heat source model, which was created by Goldak et al. [6]. One of its advantages is that it can withstand a variety of fusion welding procedures. Due to the highly concentrated heat source, mesh refinement is required along the entire welding route, which increases the computational cost of welding analysis using FEA.

Accurately predicting residual stresses in welding sequences is particularly challenging due to the local high temperature, temperature dependence of material properties, and moving heat source involved in welding. Temperature-dependent parameters from the literature are used to account for this complexity [7]. Furthermore,

*** Corresponding author:** Chouaib Zeghida, ***E-mail address:*** *c.zeghida@univ-soukahras.dz*

it is essential to account for the temperature dependency of material properties since the welding process experiences a wide temperature range. The use of temperature-independent properties may lead to significant errors in the predicted results [8]. thus, it should be highlighted the factors influencing residual stress and distortion levels in welded pipes and point out the importance of carefully selecting welding sequences and optimizing welding parameters to minimize these effects [9-10].

To analyse the thermomechanical behaviour and evaluate residual stresses in stainless steel (AISI-304), this investigation employs thermal elastoplastic analysis using finite element techniques. By using this method, we can simulate and study the temperature and stress distribution around the welded joint and evaluate the component's structural integrity including the effect of residual stress based on our past works [11-15].

2. Thermomechanical model

2.1. Thermal transients

During the welding process, a non-uniform thermal field is created surrounding the weld, which might cause RS to develop in welded structures. To determine the thermal field, transient thermal analysis with the required boundary conditions is used. The 3D transient state heat conduction equation, which is provided below, governs the transient thermal analysis of the welding process.

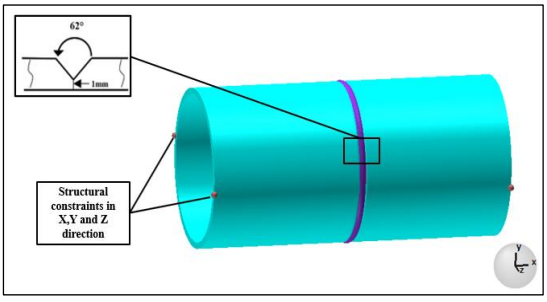

Figure 1: Graphic representations of the geometric parameters and structural boundary conditions.

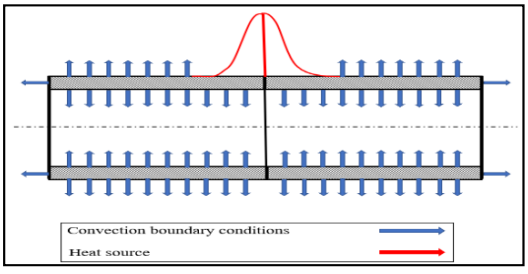

Figure 2: Schematic representations of thermal boundary conditions.

In Figure 2 boundary conditions for welding simulations naturally include both heat and mechanical factors. Free convection and radiation from the material are typically a part of the solution's thermal component. Mechanical boundary conditions are necessary for accurate deformation and stress prediction (Figure 1). Studies that

$$\frac{\partial}{\partial x}\left(K_x\frac{\partial T}{\partial x}\right)+\frac{\partial}{\partial y}\left(K_y\frac{\partial T}{\partial y}\right)+\frac{\partial}{\partial z}\left(Kz\frac{\partial T}{\partial z}\right)+Q=\rho C_P\left(\frac{\partial T}{\partial t}-v\frac{\partial T}{\partial x}\right) \quad (1)$$

Where, C_p = Specific heat, $J.kg^{-1}.K$; ρ = Mass density, $kg.mm^{-3}$; Q = Internal heat generation, $W.mm^{-3}$; v=Relative speed of heat source $mm.s^{-1}$.

The rate of heat rejection resulting from convection and radiation has been taken into account when solving the transient thermal analysis. Equation (2) defines the convection and radiation boundary conditions.

$$K_x\frac{\partial T}{\partial x}n_x+K_y\frac{\partial T}{\partial y}n_y+K_z\frac{\partial T}{\partial y}n_z+q_r+h_c\left(T-T_\infty\right)+\sigma\varepsilon F\left(T^4-T_\infty^4\right)=0 \quad (2)$$

Where, h_c= heat transfer coefficient (convection), $W.m^{-2}.K$; k= Thermal conductivity, $W.m^{-1}.K$; q= heat flux, $W.m^{-1}$; σ= Stefan-Boltzmann constant, $5.68x10^{-8}W.m^{-2}.K^4$; F= configuration factor; and n_x , n_y and n_z are the direction cosines of the boundary.

As indicated in Figure 1, we employed two cylinders in our simulation with a wall thickness of 6 mm, a length of 300 mm, and an inner diameter of 150 mm.

altered the mechanical boundary conditions and discovered noticeably varied material responses have been published [16].

2.2 Modeling of heat source

A moving heat source is a type of heat transfer phenomenon that can be applied to a variety of technical tasks, including welding. By figuring out the temperature distribution and cooling rate utilizing theoretical solutions to this problem, engineers may be able to better understand the impacts of heat input and the performance of the finished product. These solutions have applications in welding for determining the microstructure, joint strength, residual stresses, cold cracking, size of the heat-affected zone (HAZ), and deformation. The equations below state the double ellipsoid heat source model, which best describes the heat source for arc welding:

» *For the front heat source [6]:*

$$Q(x,y,z,t)=\frac{6\sqrt{3}f_f Q_w}{a_f bc\pi\sqrt{\pi}}e^{-3x'^2/a_f^2}e^{-3y'^2/b^2}e^{-3z'^2/c^2} \quad (3)$$

» *For the rear heat source [6]:*

$$Q(x,y,z,t)=\frac{6\sqrt{3}f_r Q_w}{a_r bc\pi\sqrt{\pi}}e^{-3x'^2/a_r^2}e^{-3y'^2/b^2}e^{-3z'^2/c^2} \quad (4)$$

Where x, y, and z are the welded pipe's local coordinates, and are parameters that indicate the proportion of heat deposited in the front and rear portions, respectively. Note that + = 2.0. The welding heat source's power is . Calculations can be made based on the welding current, arc voltage, and arc efficiency. It is assumed that the TIG welding technique has an arc efficiency η of 80%.

Affecting the characteristics of the welding heat source are parameters , , b and c. Under the welding requirements, the heat source's specifications can be changed to produce the necessary melted zone.

The most efficient way to simulate arc operations is to use the approach in Figure 3.

The parameters for the welding process and the heat source are displayed in Tables 1 and 2, respectively

2.3 Mechanical analysis

The elastic-plastic analysis presented in this part makes use of thermal histories derived from the previous transient thermal analysis to forecast thermal stresses and strains. In the static mechanical

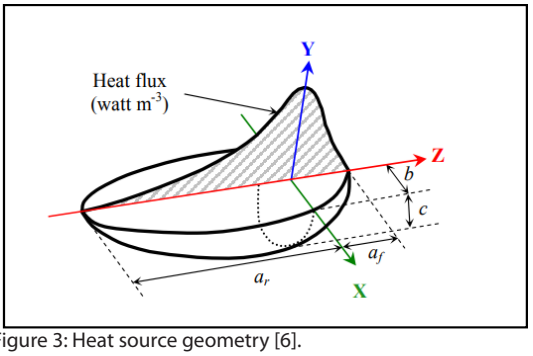

Figure 3: Heat source geometry [6].

Table 1: Goldak heat source specifications.

Parameters	Value
Length of front ellipsoidal, a_f, [mm]	2
Length of rear ellipsoidal, a_r [mm]	5
Width of heat source, 2b [mm]	6.6
Depth of heat source, c [mm]	5
Fraction of heat in front ellipsoidal, f_f	1.25
Fraction of heat in rear ellipsoidal, f_f	0.75

Table 2: Parameters of the welding process.

Parameters	Value
Welding voltage, (Volts)	12.5
Welding current, (Amperes)	120
Welding speed, v (mm.s^{-1})	3
Welding process efficiency, η (%)	80

analysis, thermal loads are represented as being comparable to body force. A specific route obtained from the prior transient thermal study was used to determine inputs for the structural analysis. Then, using incremental stress-strain relationships as stated in Equation (5), the resultant stresses and strains were determined.

$$d\varepsilon = d\varepsilon^I + d\varepsilon^p + d\varepsilon^T \quad (5)$$

Where, $d\varepsilon$ total strain; $d\varepsilon^I$, $d\varepsilon^p$ and $d\varepsilon^T$ are the elastic strain, plastic strain, and thermal stress respectively.

2.4 Material model

In welding, the type of steel used can have a significant impact on the quality of the weld and the overall durability of the finished product. In our simulation, we have utilized stainless steel (AISI 304) for welding applications due to its unique properties and benefits. AISI 304 is a commonly used stainless

Table 3: Material Properties and Their Dependence on Temperature [17].

Temperature [°C]	Thermal conductivity [N/(s. K)]	Specific heat capacity [mm²/(s².°C)]	Expansion coefficient [1/°C]	Young's modulus [GPa]
20	15.7	$5.1x10^8$	$1.6x10^{-5}$	200
100	16.8	$5.25x10^8$	$1.7x10^{-5}$	195
200	17	$5.41x10^8$	$1.8x10^{-5}$	190
400	21	$5.72x10^8$	$1.9x10^{-5}$	180
600	23.5	$6.04x10^8$	$2x10^{-5}$	150
800	26.5	$6.3x10^8$	$2.05x10^{-5}$	128
1000	29.2	$6.48x10^8$	$2.12x10^{-5}$	70
120	32.2	$6.73x10^8$	$2.2x10^{-5}$	15
1400	35.1	$6.91x10^8$	$7x10^{-6}$	10
1500	36.2	$7x10^8$	$0.1x10^{-6}$	2

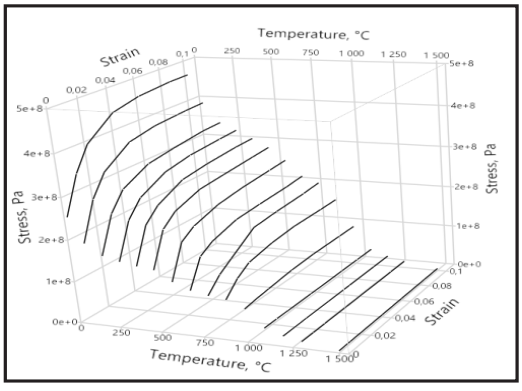

Figure 4: Flow stress for T= 20 to 1500°C [17].

steel alloy that contains both chromium and nickel, making it highly resistant to rust, corrosion, and staining. This combination of properties makes it an excellent choice for welding applications that require high strength, durability, and resistance to harsh environments. Additionally, AISI 304's low carbon content makes it more resistant to sensitization and ensures excellent weldability. The material properties of AISI 304 were taken from [17], the material Properties and Their Dependence on Temperature are given in Table 3 and Figure 4.

2.5 Mesh modeling

To accurately capture the high temperature and flux gradients present in the fusion zone (FZ) and heat-affected zone (HAZ), careful consideration of mesh size and refinement is necessary. In this regard, a relatively fine mesh is employed within a distance of 30 mm on both sides of the weld line (WL), where the most significant thermal effects are expected. This fine mesh allows for a more precise representation of the temperature distribution in these critical areas. As the distance from the WL increases, the element size is progressively enlarged to account for the diminishing impact of the

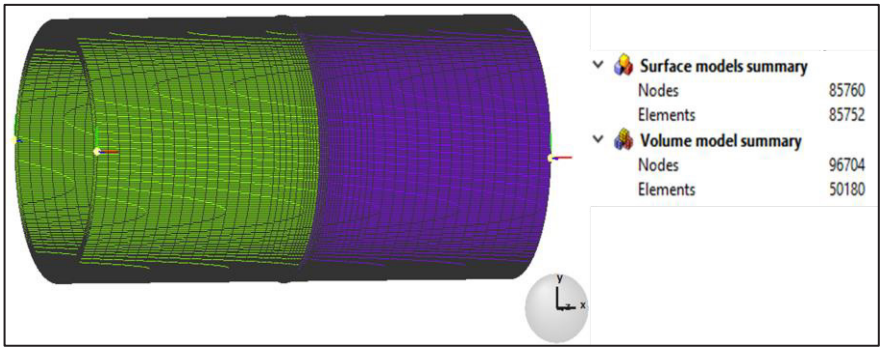

Figure 5: 3D FE mesh based on sensitivity analysis.

welding process.

To maintain consistency in the weld direction, a constant element size of 1 mm is utilized. This ensures that the welding effects are adequately captured throughout the entire length of the weld. In the transverse direction, where the HAZ spans approximately 30 mm on each side of the WL, an element size of 1.96 mm is employed. This slightly larger element size strikes a balance between computational efficiency and capturing the thermal behaviour within the HAZ region accurately.

The selection of the mesh parameters mentioned above is based on a comprehensive mesh sensitivity analysis performed through successive mesh refinements. By systematically refining the mesh and evaluating the resulting solutions, it was determined that the maximum temperature attained during the analysis serves as a key criterion for optimizing the mesh. It was observed that further increasing the maximum temperature would not be achieved by exceeding 85752 elements. Figure 5 illustrates the finite element mesh used in the analysis, showcasing the spatial distribution of the elements throughout the domain.

3. Results and Discussion

When it comes to welding, the number of passes plays a crucial role in determining the strength and quality of the weld joint. One-pass welding refers to a technique where the entire weld joint is completed in a single run. This method is often used for thin materials or applications where speed is a priority. On the other hand, four-pass welding involves dividing the weld joint into four separate passes, each applied sequentially. This approach is commonly employed when dealing with thicker materials or when superior strength and durability are paramount (see Figure 6).

The FE application has recently grown in popularity within the industry. One of the newest FE programs currently available is Simufact-Welding. For the analysis and improvement of welding processes, it is a specially designed software program. After the thermal analysis, Simufact-welding performs a mechanical analysis to simulate the mechanical response of the welded structure. This analysis considers the thermal history obtained from the thermal analysis, along with the material properties and boundary conditions. The mechanical analysis calculates the stresses and strains during and after the welding process, including the residual stresses. Simufact-welding provides tools to evaluate and visualize the residual stresses in the welded structure. The software can generate contour plots, 3D stress distributions, and residual stress profiles along specified locations. [18].

It's important to note that Simufact-welding offers a range of advanced features and options that allow users to customize the simulation methodology according to their specific requirements. The software incorporates various numerical techniques and algorithms to accurately predict the residual stresses induced by the welding process.

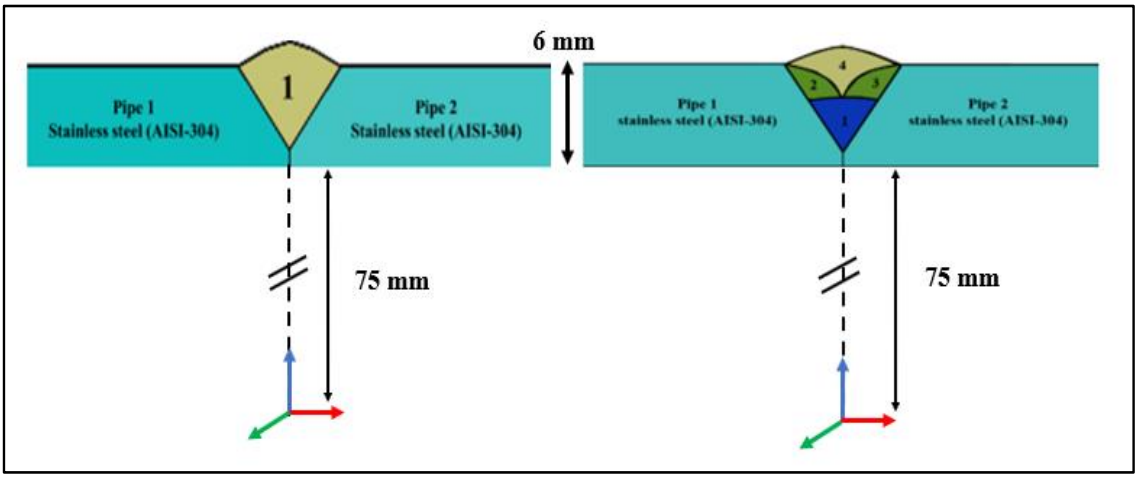

Figure 6: Zoom to the vicinity of one and multi-pass welding in a butt joint.

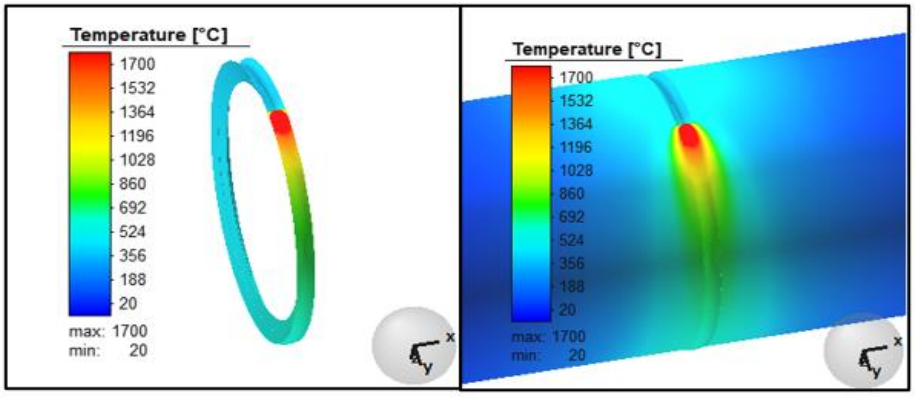

Figure 7: Temperature change in Robot and complete model, [°C].

Many scientists have used commercial software to extensively predict the distortion caused by the heat of robotic welding. FEA is currently the preferred tool for welding simulation. After the completion of the welding simulation, the mechanical, thermal, and total distortion results were discussed in the following sections.

3.1. Temperature distribution

Therefore, being able to forecast transient temperature fields is essential because it allows us to determine whether safety-critical welded components will be able to function satisfactorily for the duration of their intended service lives. Temperature change in Robot, the complete model, and the peak temperature at process time 328sec are presented in Figure (7–8). Figure 9 presents the

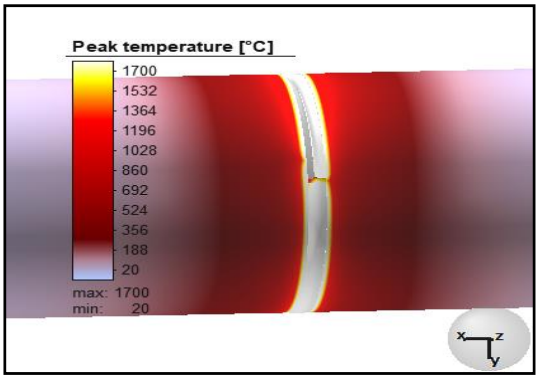

Figure 8: Peak temperature change, [°C].

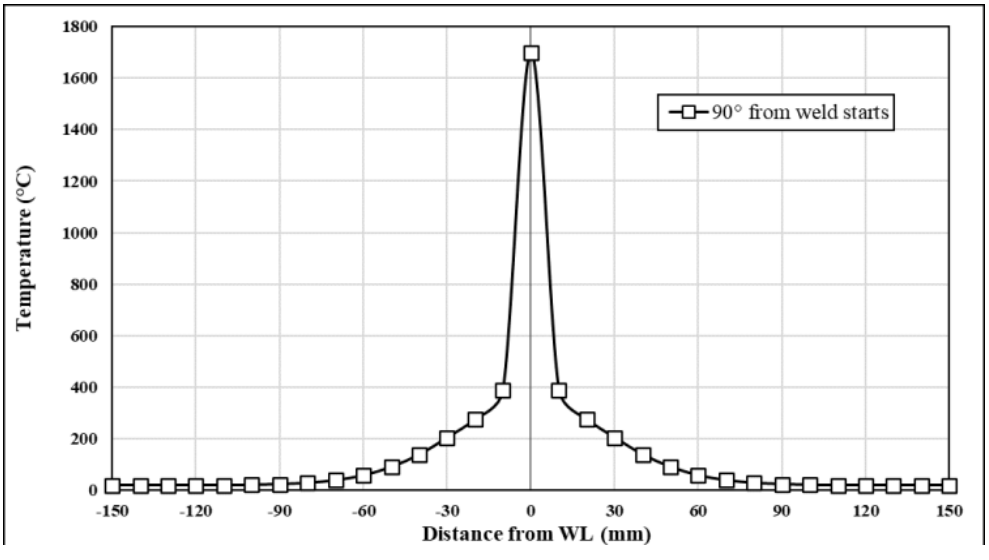

Figure 9: Axial temperature distribution at 90° from weld start, [C°].

axial temperature distribution at 90° from weld start.

3.2 Angular distortion

To fuse the materials during welding, the junction is typically heated. The expansion and contraction brought on by this heat. Distortion may occur if the heating and cooling are unequal, the residual stress is what causes this deformation. Only the change in weld area volume and subsequent movement of the material after it hardens and cools to room temperature can be used to determine the extent of the thermal stress applied to the material, and Figures (10-11) confirm that.

When the angles between the welded components are changed by contraction, angular distortion occurs. Due to the top's bigger weld pool than the bottom, the contraction is more noticeable, as shown in Figure 12.

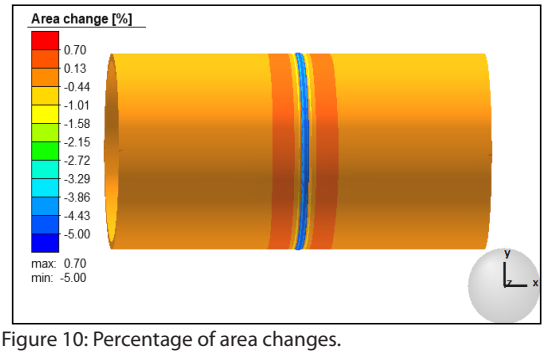

Figure 10: Percentage of area changes.

3.3 Residual stress

Residual stresses in welded joints primarily developed due to differential heating, peak temperature, and cooling at any moment during welding. As shown in Figure 11, the amount of residual stress after the welding simulation showed vast differences.

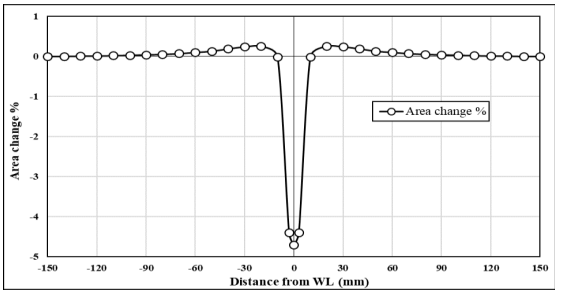

Figure 11: Axial distortion, [%].

The distribution of residual stresses differs between one-pass welding and multi-pass welding (see Figure 13). In one-pass welding, where the entire weld joint is completed in a single run, the distribution of residual stresses tends to be more concentrated near the weld. This concentration is primarily due to the rapid heating and cooling of the material in a relatively short time frame. As a result, one-pass welding can lead to higher localized residual stresses near the weld zone as shown in Figure 14.

By referring to Figure 14, multi-pass welding, which involves dividing the weld joint into multiple passes, allows for better stress redistribution. With each pass, the heat input and subsequent cooling occur over a smaller area, enabling more gradual temperature changes. This gradual approach helps to alleviate the build-up of excessive thermal stresses and allows for better stress relaxation throughout

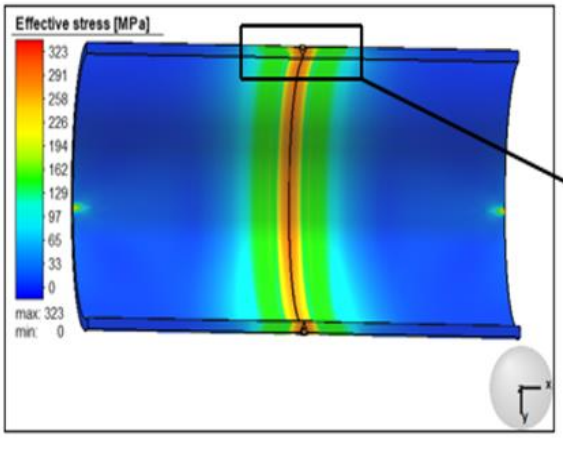

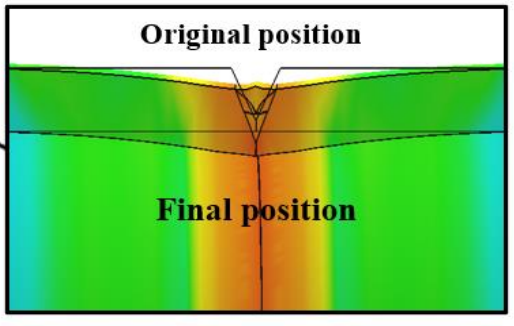

Figure 12: Effective stress change, [MPa].

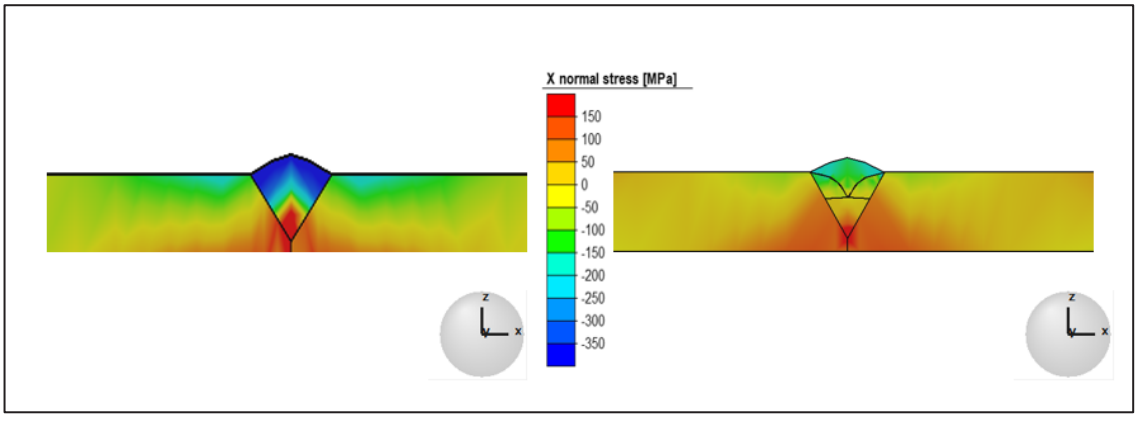

Figure 13: Axial residual stress plots on the wall thickness for one and multi-pass welding.

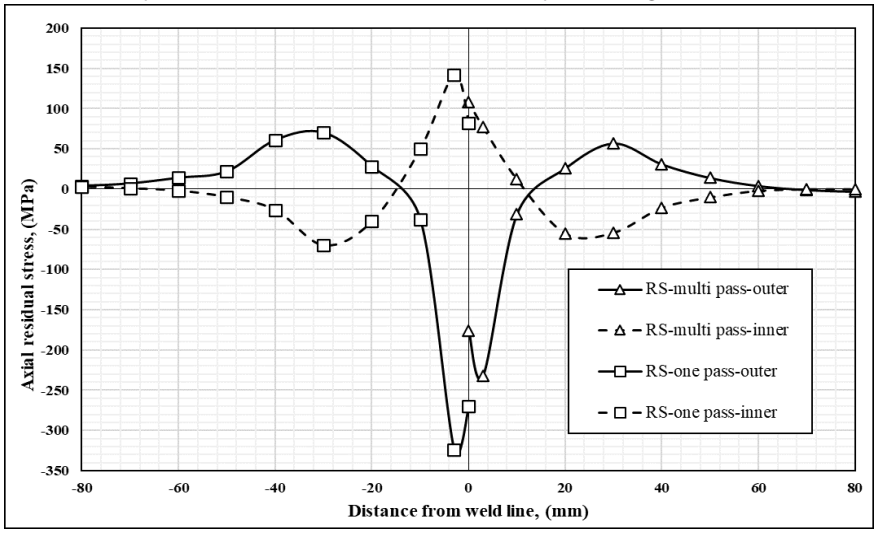

Figure 14: Axial residual stress distribution for one and multi-pass welding (outer and inner surface).

the welded structure. As a result, multi-pass welding tends to exhibit a more uniform distribution of residual stresses across the welded joint.

On the outer and inner surfaces of the cylinders, the compressive and tensile axial stress fields, respectively, are shown in and close to the weld zone. This is explained by the differing temperature profiles on the cylinders' inner and outer surfaces. Tensile and compressive residual stress fields are produced on the inner and outer surfaces, respectively, along the weld line, as a result of varying shrinkage patterns through the wall thickness caused by distinct temperature gradients (WL), as shown in Figure (15-16).

Axial stress distributions on the outer and inner surface of the cylinders at various cross-sections from the weld start location are shown in Figure (17-18).

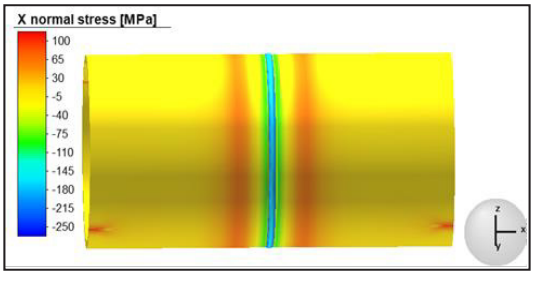

Figure 15: Axial residual stress distribution (outer surface).

By referring to Figure 17, high compressive stresses appear near the WL. After 14 mm on each side of the WL, the compressive residual axial stresses near the WL vanish to zero. Beyond this, the tension is found to switch from compressive to tensile. Nearly 70 mm distant from the WL, these low-magnitude tensile

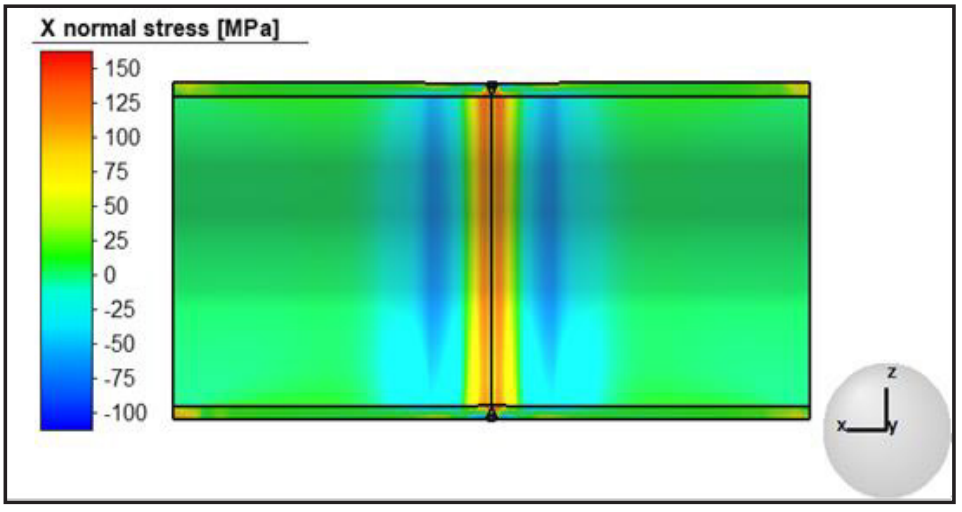

Figure 16: Axial residual stress plots on the inner surface.

stresses once more approach a zero value.

For cylinder inner surfaces at various cross sections from the weld start position, the high tensile stresses near the WL approach zero and then reverse to lower compressive residual stresses at 14 mm, increasing to an almost constant value of zero at 70 mm as shown in Figure 18. The position around the circumference has only a minimal influence on axial stresses. Axial residual stresses on the outer and inner surfaces for four different cross sections (60°, 120°, 180°, and 240°) are virtually of the same magnitude and trend, as shown in Figures 17 and 18.

3.4 Effect of residual stress on the in-service reliability evaluation

The axial residual stress distributions through the thickness of a cylinder's wall at the weld centreline are depicted in Figure 19. These residual stresses exhibit a pattern of compressive stress on the outer surface of the cylinder and tensile stress on the

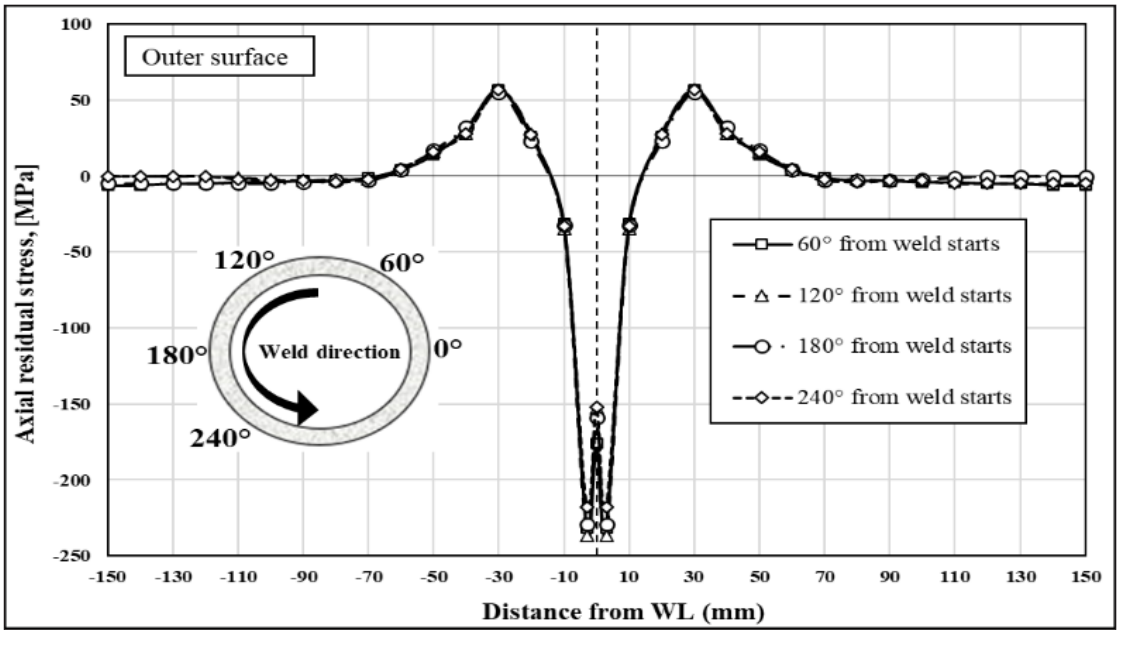

Figure 17: Axial residual stress plots on the outer surface.

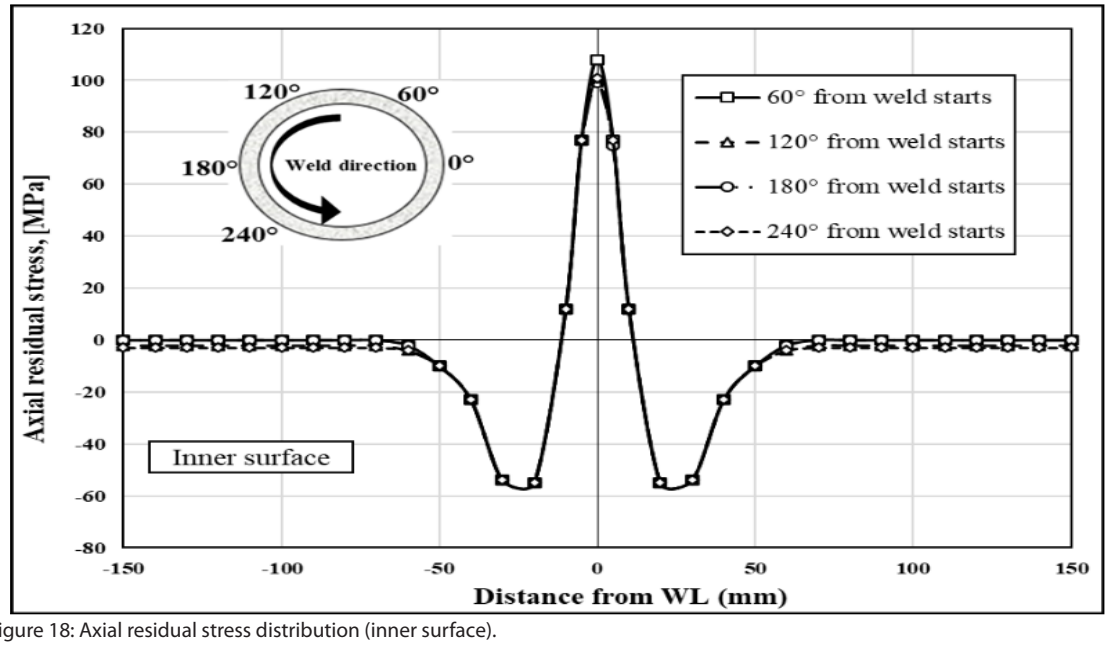

Figure 18: Axial residual stress distribution (inner surface).

inner surface. The weld region typically exhibits the highest residual stress magnitudes due to the extreme temperature gradients experienced during welding. Rapid temperature changes and thermal cycling result in non-uniform cooling and thermal contraction, causing a net bending moment at the weld. As a result, tensile reaction stresses are present on the inner surface of the cylinder at the weld's root, while compressive stresses are present on the outer surface.

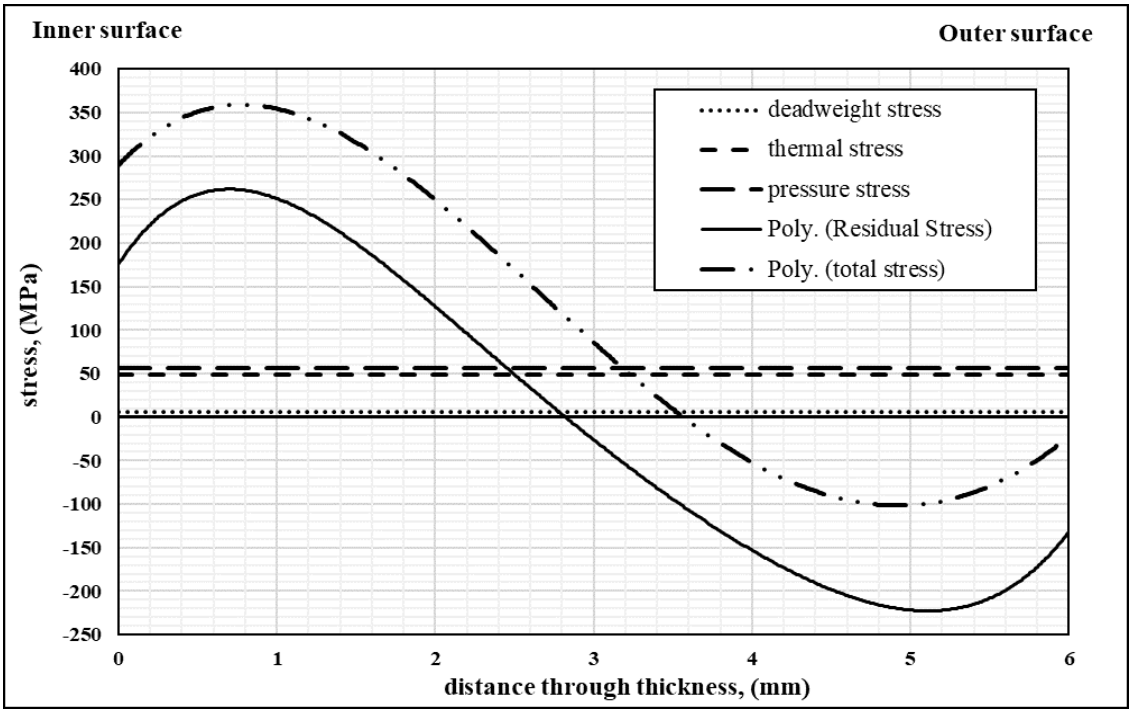

Figure 19: Axial residual stress distribution through the wall thickness at the weld centreline.

Experience has shown that austenitic piping is susceptible to IGSCC in the weld root area under BWR service conditions. The present state of knowledge attributes three factors that must be present simultaneously to causing IGSCC. These factors are (1) a corrosive environment, (2) a material susceptible to cracking, and (3) a tensile state of stress.

1. A corrosive environment is a critical factor in IGSCC. Environments containing corrosive species, such as chlorides, sulphides, or alkaline solutions, can accelerate crack growth by chemically attacking the grain boundaries.

2. Not all materials are equally susceptible to IGSCC. Certain alloys and materials with specific microstructures or chemical compositions are more prone to this type of cracking. Grain boundaries with a high degree of sensitization or segregation can be particularly susceptible.

3. The presence of tensile stress acts as a driving force for crack initiation and propagation. Tensile stresses can arise from various sources, such as residual stresses from welding, thermal cycling, or mechanical loading.

The operating stresses, as depicted in Figure 19, and the input values assigned to SCC parameters and pipe loading are given in Table 4; encompass a range of factors that impose mechanical forces upon the pipe cross-section. These stresses arise from multiple sources, including internal pressure, dead-weight loading, and the effect of thermal expansion, which results in a bending moment exerted on the pipe. The internal pressure within the pipe creates a force that seeks to expand the pipe's walls outward. This pressure-induced stress is a crucial consideration in designing a robust and reliable piping system.

In addition to internal pressure, dead-weight loading adds to the overall stress experienced by the pipe. This refers to the weight of the pipe itself and any other components or substances it carries, such as fluids or structural attachments. The gravitational pull on these elements places a downward force on the pipe, leading to additional stresses. Furthermore, the thermal expansion introduces a unique form of stress. When subjected to temperature variations, the pipe material expands or contracts. This expansion can induce a bending moment, causing the pipe to deform. The resultant stress from this thermal expansion bending moment adds to the overall mechanical strain experienced by the pipe.

The reliability model, which was developed in our previous work [15], is adapted specifically for evaluating the probability of failure in AISI 304 piping. This model incorporates the estimated damage and utilizes probabilistic methods to assess the reliability of the piping system. By considering the uncertainties and variability associated with the inputs and the welding residual stress, the reliability model provides insights into the likelihood of failure under given conditions (Table 4).

Due to the low probability of pipe failure, appropriate statistical methods, such as the Monte Carlo Simulation (MCS), are used to obtain sufficient data for reliability analysis.

Fig. 17 shows, the cumulative leakage

Table 4: Input values of SCC parameters and pipe loading [15].

Outside diameter [mm]	162
Wall thickness [mm]	6
Initial flaw distribution [mm]	Log-normal distribution Deterministic flaw depth = 0.025 Mean flaw length = 3.2 Shape parameter = 0.85
Pipe loading values [MPa]	Stress due to cold deadweight = 6.55 Stress due to thermal = 48.74 Operating pressure = 9.17 Stress due to operating pressure = 56.60 Stress due to dwt+thml+op.pres = 111.89
SCC Parameters	O2 at start-up [ppm] = 8.00 O2 at steady state [ppm] = 0.20 Temp. at steady state [°C] = 293.33 Heat up (38-260 [°C]), Time [hrs] = 5.00 Coolant conductivity [µS/cm] = 0.20
Welding residual stress [MPa]	Refer to Figure 19 for further clarification

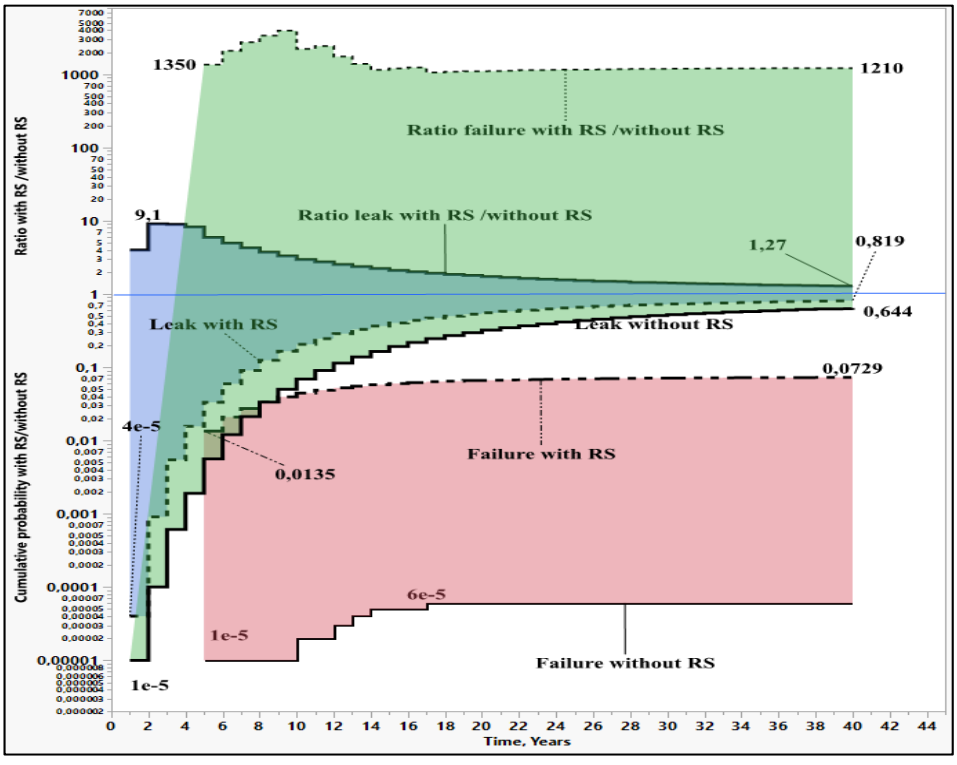

Figure 20: Effect of residual stress on the in-service reliability prediction.

probabilities of the cases treated. The results are given for both with and without residual stress. In the case of including residual stress, a leak should occur after two years of operation (i.e. the cumulative probability of leakage approaches this). While it is important to keep in mind the conservatism of the analysis, this result is nevertheless reasonably consistent with some field observations [14-15]. In the case, of low residual stress, the corresponding leakage probability presents only 1/9 of the value one considering the effect of residual stress. At the end of life, the ratio of leak cumulative probability with and without residual stress is 1,27 and the ratio of failure cumulative probability with and without residual stress is 1210.

3.5 Yield stress

Considering the thorough analysis of total distortion and residual stress in austenitic pipe's butt joints, valuable insights can be drawn regarding the impact of multi-pass welding on the yield strength of the material. The findings indicate that the total distortion resulting from the welding process does not exert a significant influence on the yield strength of the material. This suggests that despite the occurrence of distortion during the multi-pass weld on the tubular butt junction, the material's ability to withstand deformation and retain its mechanical integrity remains largely unaffected. Consequently, the structural strength and performance of the welded joint are not substantially compromised by the observed distortion. These conclusions provide reassurance regarding the reliability and suitability of the chosen welding technique for austenitic pipes, as it demonstrates that the induced total distortion does not compromise the material's inherent yield strength and structural integrity.

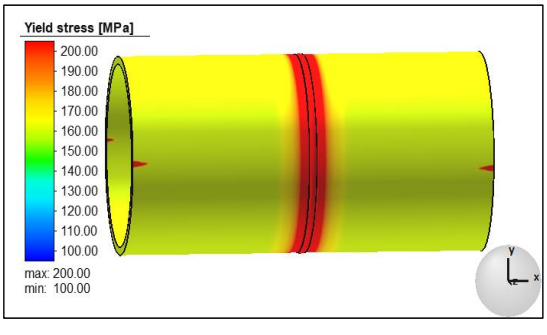

Figure 21: Yield stress change, [MPa].

4. Conclusions

Based on the total distortion and residual stress analysis of the austenitic pipes butt joint, it can be concluded that the yield strength of the material is not significantly affected by the total distortion that occurred during the multi-pass weld on the tubular butt junction. However, the welded metal has higher residual stress compared to other structural components. There is also significant axial residual stress along and around the weld line, as well as on the inner and outer surfaces of the pipe, respectively. These stresses can be compressive or tensile, depending on their location. Moreover, it was found that a multi-pass weld can enhance joint strength, weld thicker sections, and temper the previously deposited weld. This results in a microstructure with less residual stress. Therefore, it is recommended to use a multi-pass weld technique for butt joint welding of austenitic pipes. These findings are essential for the design and fabrication of pipelines and other similar structures, as they provide valuable information that can aid in the optimization of the welding process and improve the overall quality and durability of the welded joints.

References

[1] P. J. Withers and H. K. D. H. Bhadeshia, "Residual stress. Part 1 – Measurement techniques," Materials Science and Technology, vol. 17, no. 4, pp. 355–365, Apr. 2001, doi: 10.1179/026708301101509980.

[2] S. A. Tsirkas, P. Papanikos, and T. Kermanidis, "Numerical simulation of the laser welding process in butt-joint specimens," Journal of Materials Processing Technology, vol. 134, no. 1, pp. 59–69, Mar. 2003, doi: 10.1016/S0924-0136(02)00921-4.

[3] W. Perret, "Welding Simulation of Complex Automotive Welded Assembly Possibilities and Limits of the Application of Analytical Temperature Field Solutions", ISBN3981594401 BAM,2013, 184 pages.

[4] W. Perret, C. Schwenk, M. R. Ethmeier, T. R. Raphael, and U. Alber, "Case Study for Welding Simulation in the Automotive Industry," Welding in the World, vol. 55, no. 11–12, pp. 89–98, Nov. 2011, doi: 10.1007/BF03321546.

[5] H. D. Hibbitt and P. V. Maikal, "A numerical, thermo-mechanical model for the welding and subsequent loading of a fabricated structural". doi.org/10.1016/0045-7949(73)90043-6.

[6] J. Goldak, A. Chakravarti, and M. Bibby, "A new finite element model for welding heat sources," Metallurgical and Materials Transactions B, vol. 15, no. 2, pp. 299–305, Jun. 1984, doi: 10.1007/BF02667333.

[7] C. Zeghida, M. A. Belyamna, S. Tlili, and A. Guedri, "The Effect of Induction Heating Stress Remedies on piping reliability," Procedia Structural Integrity, vol. 41, pp.384–393, 2022, doi: 10.1016/j.prostr.2022.05.044.

[8] L. E. Lindgren, "Finite element modeling and simulation of welding. part 2: improved material modeling," Journal of Thermal Stresses, vol. 24, no. 3, pp. 195–231, Mar. 2001, doi: 10.1080/014957301300006380.

[9] N. Moslemi, B. Abdi, S. Gohari, I. Sudin, N. Redzuan, A. Ayob, M. Ahmed, S. Rhee, C. Burvill, "Influence of welding sequences on induced residual stress and distortion in pipes Construction and Building Materials," Volume 342, Part A, 2022, doi. org/10.1016/j.conbuildmat.2022.127995.

[10] M. Ghafouri, A. Ahola, J. Ahn, T. Björk, "Welding-induced stresses and distortion in high-strength steel T-joints: Numerical and experimental study," Journal of Constructional Steel Research, Volume 189, 2022, doi.org/10.1016/j.jcsr.2021.107088.

[11] A. Guedri, A. Zeghloul and B. Merzoug, "Reliability analysis of BWR piping including the effect of Residual Stresses", International Review of Mechanical Engineering, Vol. 3(5), pp. 640-645, 2009

[12] A. Guedri, Y. Djebbar, Moe. Khaleel and A. Zeghloul, "Structural Reliability Improvement Using In-Service Inspection for Intergranular Stress Corrosion of Large Stainless-Steel Piping," In Applied Fracture Mechanics, Alexander Belov (Ed.), pp.331-358, 2012, doi: 10.5772/48521.

[13] A. Guedri, "Reliability analysis of stainless-steel piping using a single stress corrosion Cracking Damage Parameter", International Journal of Piping and Pressure Vessel, Vol. 1(11), pp.111–112, 2013, doi.org/10.1016/j.ijpvp.2013.03.011.

[14] A. Guedri, "Effects of remedial actions on small piping reliability", Journal of Risk and Reliability, Proceedings of the IMechE (Part O), Vol.227(2), pp.144-161, 2013, doi. org/10.1177/1748006X13477798.

[15] M. A. Belyamna, C. Zeghida, S. Tlili, and A. Guedri, "Piping reliability prediction using Monte Carlo simulation and artificial neural network", Procedia Structural Integrity, Vol. 41, pp.372-383, 2022, doi.org/10.1016/j.prostr.2022.05.043.

[16] K. Y. Bae and S. J. Na, "A Study of the Effect of Pre-Straining on Angular Distortion in One-Pass Fillet Welding Incorporating Large Deformation Theory," Proc. Inst. Mech. Eng. Part B J. Eng. Manuf., vol. 209, no. 5, pp. 401–409, Oct.1995, doi: 10.1243/PIME_PROC_1995_209_099_02

[17] Voß, Olaf. "Investigation of relevant influencing variables on numerical welding simulation". Dissertation, Technical University of Braunschweig, 2001. No strain-rate dependency considered, Updated 12.01.2012 (in German).

[18] Simufact Welding, https://www.simufact.com/simufactwelding-welding-simulation.html.